Contents lists available at ScienceDirect

Biomaterials

journal homepage: www.elsevier.com/locate/biomaterials



Transdermal colorimetric patch for hyperglycemia sensing in diabetic mice



^{a,b,1}, Jinqiang Wang^{a,b}, Zhaowei Chen^{a,b}, Guojun Chen^{a,b}, Di Wen^{a,b}, Zejun Wang^{a,b,1}, Amanda Chan^{a,b}, Zhen Gu^{a,b,c,d,*}

- ^a Department of Bioengineering, University of California, Los Angeles, CA, 90095, United States
- ^b California NanoSystems Institute, University of California, Los Angeles, CA, 90095, United States
- ^c Jonsson Comprehensive Cancer Center, University of California, Los Angeles, CA, 90095, United States
- d Center for Minimally Invasive Therapeutics, University of California, Los Angeles, CA, 90095, United States

ARTICLE INFO

ABSTRACT

Keywords: Glucose sensor Microneedle Glucose-responsive Colorimetric sensor Enzyme biomineralization The integration of sampling and instant metabolite readout can fundamentally elevate patient compliance. To circumvent the need for complex in-lab apparatus, here, an all-in-one sampling and display transdermal colorimetric microneedle patch was developed for sensing hyperglycemia in mice. The coloration of 3,3',5,5'-tetramethylbenzidine (TMB) is triggered by the cascade enzymatic reactions of glucose oxidase (GOx) and horseradish peroxidase (HRP) at abnormally high glucose levels. The HRP in the upper layer is biomineralized with calcium phosphate (CaP) shell to add a pH responsive feature for increased sensitivity as well as protection from nonspecific reactions. This colorimetric sensor achieved minimally invasive extraction of the interstitial fluid from mice and converted glucose level to a visible color change promptly. Quantitative red green and blue (RGB) information could be obtained through a scanned image of the microneedle. This costless, portable colorimetric sensor could potentially detect daily glucose levels without blood drawing procedures.

1. Introduction

Diabetes mellitus refers to an incurable chronic disease characterized by abnormally high blood-glucose levels, known as hyperglycemia [1]. Diagnostic devices for home-based daily monitoring of glucose level can aid diabetes patients in seeking timely treatments to prevent symptoms including nephropathy, high blood pressure, and stroke [2]. Minimally invasive sample collecting modules and diagnostic information-display modules are two fundamental factors for developing a portable, cheap and simple to use glucose sensor.

The existing glucose level measurements require invasive blood sampling [3]. As a painless alternative, strategies using a microneedle array patch have been extensively adopted for extracting [4,5] and detecting metabolites [6] or delivering therapeutic drugs [7-9] in the interstitial fluid, which is the extracellular fluid surrounding tissue cells that possesses similar composition of clinically important biomarkers to blood, including glucose levels [10].

Colorimetric bio-sensing is favorable for on-site analysis and pointof-care diagnosis, without the need for complex in-lab apparatus [11,12]. Integration of a dual enzymatic system that consists of glucose oxidase and peroxidase could achieve rapid colorimetric sensing of glucose [13]. Glucose oxidase [14,15] is responsible for transforming glucose into chemical signals of gluconic acid and H₂O₂. Peroxidase [16-18], thereafter, can catalyze substrates including 3,3',5,5'-tetramethylbenzidine (TMB), 2,2'-azino-bis(3-ethylbenzothiazoline-6-sulfonic acid) (ABTS), o-phenylenediamine (OPD), and diazoaminobenzene (DAB) to generate color change visible to the naked eye in the presence of hydrogen peroxide (H₂O₂). However, enzymatic reactions are sensitive to environmental changes such as pH and digestive proteases. In this case, the byproduct gluconic acid would significantly lower the surrounding pH and inhibit HRP activity with the increase of glucose [19], which greatly decreases the sensitivity of the system. In addition, current colorimetric sensors are mainly dependent on in-solution reactions, which is a major issue for storage and transportation.

Herein, we describe a poly(vinyl alcohol) (PVA)-based double layer microneedle patch, achieving both in situ dermal sample collection and instant color display. The bottom needle layer is embedded with glucose oxidase, while the upper layer is immobilized with biomineralized HRP (calcium phosphate-encapsulated HRP, HRP-CaP) and TMB. Upon glucose challenge, glucose oxidase selectively converts glucose into gluconic acid and H₂O₂, thereby lowering the local pH to free HRP from HRP-CaP and induce the catalytic oxidation of the TMB substrate in the

^{*} Corresponding author. Department of Bioengineering, University of California, Los Angeles, CA, 90095, United States. E-mail address: guzhen@ucla.edu (Z. Gu).

¹ Z.W. and H.L. contributed equally.

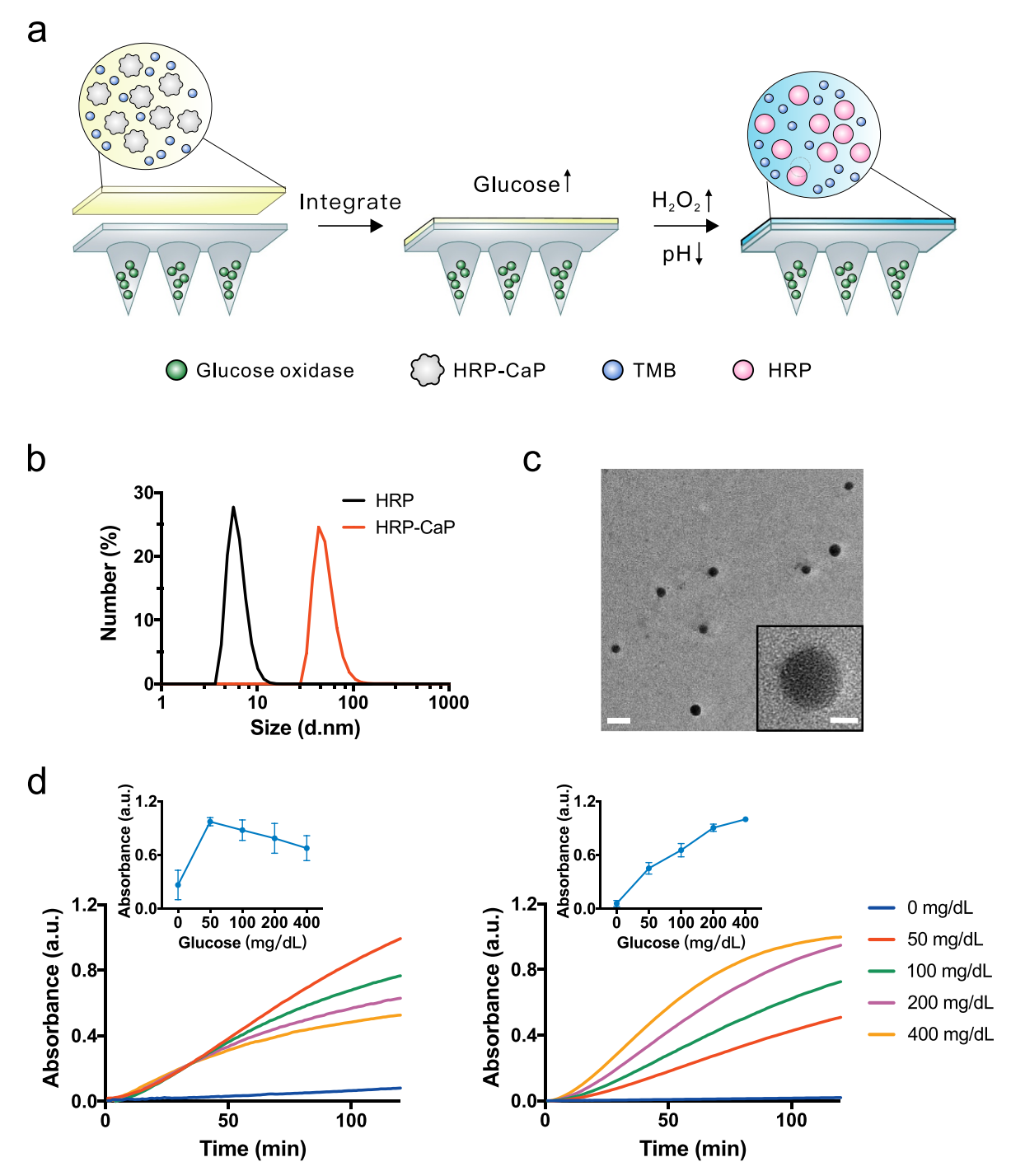


Fig. 1. HRP-CaP characterization and enzymatic activity study. a) Schematic of the glucose-responsive colorimetric microneedle sensing platform triggered by both pH decrease and H_2O_2 generation. b) Dynamic light scattering (DLS) size measurements of HRP and HRP-CaP in water. c) TEM image of HRP-CaP particles. Scale bar, 100 nm (inset: 20 nm). d) A representative normalized kinetic curve of TMB color change in solutions supplemented with GOx and 50–400 mg/dL glucose in the presence of HRP (left) or HRP-CaP (right). Inset is the endpoint (2h) absorbance at 650 nm, results are expressed as mean \pm SD (n = 3). (For interpretation of the references to color in this figure legend, the reader is referred to the Web version of this article.)

presence of hydrogen peroxide (Fig. 1a). It features a dual responsive mechanism to increase sensitivity accompanied by a layer of protection from nonspecific oxidation. The incorporation of a biocompatible inorganic shell maintained the intrinsic catalytic efficiency of the natural enzymes with improved robustness. The costless (5 cents for each test) microneedle sensor could distinguish the glucose level between 50 mg/dL and 400 mg/dL within 30 s *in vitro* and the hyperglycemia occurrence in mice could be recognized with the naked eye within 4 min after insertion.

2. Materials and methods

2.1. Preparation of biomineralized HRP formulation

Briefly, 1 mg of HRP was dissolved directly in 1 mL of DMEM medium and kept for three days or longer to reach equilibrium. An additional 3.2 μ L of CaCl₂ (1 M) was introduced to DMEM (with 1.8 mM Ca²⁺) to reach a final Ca²⁺ concentration of 5 mM and was incubated at 37 °C under 5% CO₂ for 24 h. The reaction tubes were sealed with

aluminum foil with holes to adjust the system-environment substrate exchange. The HRP-CaP particles was purified from DMEM and washed three times with water by centrifugal ultrafiltration (100k MWCO, 14000 g, 10 min) followed by resuspension in 1 mL water and kept at 4 $^{\circ}\text{C}$ before use (0.3 mg/mL). The 30% yield of HRP-CaP was calculated by measuring and comparing the enzymatic activity of the filtered solution to the original solution.

2.2. Fabrication of double-layer microneedle array patch

The extraction layer of the MN patch was fabricated using polydimethylsiloxane micromolds purchased from Blueacre Technology Ltd., Ireland with a round needle base of 500 um in diameter and 1500 μm in height. These needle cavities are arranged in a 10 imes 10 array with 700 µm tip-tip spacing. For preparing the extraction layer, water was first deposited onto the needle and kept under vacuum for 5 min to remove air from the cavities. Then, excess water was replaced with 0.01 mg/mL GOx solution in 1.5% PVA and kept under vacuum for another 5 min. Finally, 1.2 mL 15% PVA containing 0.1 mg/mL GOx was loaded onto the microneedle patch after removal of the excessive 1.5% PVA solution. This micromold was kept under air to dry for 48 h before peeling off the MN patch. For the display layer, 15% PVA was premixed with a final concentration of 0.5 mg/mL TMB-HCl and 0.015 mg/mL HRP-CaP, the mixture was loaded on a 2 \times 2 cm flat surface for 24 h to form a film. Subsequently, the display layer was separated from the surface, glued to the extraction layer with a brush of 15% PVA solution and allowed to dry at room temperature. After complete desiccation, each MN patch was cut into four 5 × 5 array patches with a blade.

2.3. In vivo studies using streptozotocin-induced diabetic mice

The in vivo performance of the double layer colorimetric microneedle for hyperglycemia detection was evaluated on streptozotocininduced adult diabetic mice (male C57B6, age 8 wk; Jackson Laboratory). C57BL/6J mice were used as normoglycemia control. All animal experiments were performed in compliance with an animal study protocol approved by the Institutional Animal Care and Use Committee at University of California, Los Angeles. For in vivo sensing experiments, the mice were shaved one day before the colorimetric patch application. To evaluate the sensing ability of the MN, blood glucose level of the mice were first recorded using the Accu-Chek Aviva blood glucose meter (Roche Diabetes Care, Inc.) through the tail vein blood (\sim 3 μ L). To avoid movement, the mice were anesthetized with isoflurane during the application of the sensors. MN colorimetric patch was pressed firmly for the first 10 s, during which the shape and mechanical strength of MN were maintained for easy penetration through the epidermis. To ensure sufficient extraction of interstitial liquid to the microneedle, the sensor was softly pressed for an additional 5 min. Color change would occur in the next 5 min for hyperglycemic mice and the microneedle was eventually removed for further analysis.

2.4. RGB analysis

The microneedles were first aligned on a glass slide and color scanned with a HP OfficeJet 4650 scanner. The image was analyzed using the RGB Histogram plugin in ImageJ.

3. Results and discussion

3.1. Synthesis and characterization of biomineralized HRP (HRP-CaP)

Like many biomineralization-related proteins, HRP contains Ca²⁺ binding ligands that serve as "nucleation sites" for concentrating

cationic calcium ions and generate tiny crystals around the peptides. Eventually, the crystals assemble into spherical particles [18,20]. The mild biomineralization process is conducted in the Dulbecco's modified Eagle's medium (DMEM) containing an optimal Ca2+ concentration of 5 mM for 24 h at 37 °C with 5% CO2 (Fig. S1). The size shift from $6.2~\pm~1.4~\text{nm}$ to $51.5~\pm~14.8~\text{nm}$ was verified with dynamic light scattering (Fig. 1b) and could be distinguished by the enhanced Tyndall effect (Fig. S2). An observation of decreased zeta potential from -7.9 ± 2.5 mV to -20.3 ± 1.3 mV is attributed to the surface domination of phosphate ions and structural water (Fig. S3) [21]. Additionally. Fourier transform infrared (FTIR) spectroscopy showed that HRP-CaP particles possess distinguished characteristic peaks of inorganic phosphates [22] (P-O vibration) at 1000-1100 cm⁻¹ while retaining the CONH- (amide I) and amide II vibrations from HRP at 1655 and 1542 cm⁻¹ (Fig. S4) [23]. Transmission electron microscopy (TEM) images and scanning electron microscopy (SEM) revealed the general size of the spherical particles to be around 52.5 \pm 11.0 nm (Fig. 1c and Fig. S5). To further confirm the composition of the HRP-CaP complex, elemental analysis was carried out with energy dispersive spectroscopy (EDS). Characteristic peaks at around 2.013 keV and 3.690 keV indicate the presence of P and Ca from calcium phosphate (CaP) (Fig. S6). Element composition of N and Ca was performed at the center and edge point of the particle. At the center, 67.23% of N was detected while only Ca could be identified at the edge of the particle (Fig. S7). The overall characterizations confirmed the formation of CaP encapsulated HRP core-shell complex.

To further validate the HRP enzymatic activity of the HRP-CaP complex, we compared the TMB oxidation kinetics of HRP and HRP-CaP at various pH buffer solutions (Fig. S8). HRP alone exhibited the highest activity at pH 5.6 while the activity dropped dramatically when pH approached 4 or 7. In contrast, the inorganic shell of the HRP-CaP extended the increased enzymatic activity to pH 4, suggesting a sustained and gradual dissociation profile of HRP from the inorganic shell at decreased pH. This correlation between pH and HRP-CaP activity may contribute to the enhanced sensitivity of the dual enzymatic reaction for sensing glucose level. Therefore, we next assessed the catalytic performance of HRP-CaP and HRP in vitro in the presence of TMB, GOx and different concentrations of glucose (Fig. 1d). As expected, the TMB colored substrate absorption at 650 nm for HRP alone decreased with increasing glucose levels in the range of 50-400 mg/dL. In comparison, TMB absorption readout for HRP-CaP was in positive correlation with the glucose level, facilitating a pH responsiveness to the sensor. In this regard, the CaP shell does not affect the enzymatic activity of HRP. In turn, it provides a second trigger along with H2O2 to elevate the sensitivity of glucose sensing as well as reducing the nonspecific reactions of HRP (Fig. S9).

3.2. Microneedle fabrication and characterization

Swelling-driven capillary flow is the dominant mechanism for rapid interstitial fluid extraction and effective enzymatic product diffusion. To guarantee the molecular interactions of various components and enzymatic products, the microneedle should be water absorbing while not dissolving, and possess sufficient mechanical strength for skin penetration. For the color display, aside from the properties listed above, good transparency and the ability to form fine films are also essential. PVA is a swellable and cost-effective polymer that is capable of absorbing 10–30% its own weight water within minutes and can readily form films [24–26]. Thus, we adopted PVA for the separate fabrication of the bottom and top layer utilizing a vacuum-based micromolding strategy for the microneedle layer.

A simple three-step fabrication was developed to prepare the double layer microneedle with separated enzymatic functions. In brief, the PVA-based microneedles containing GOx were first molded and

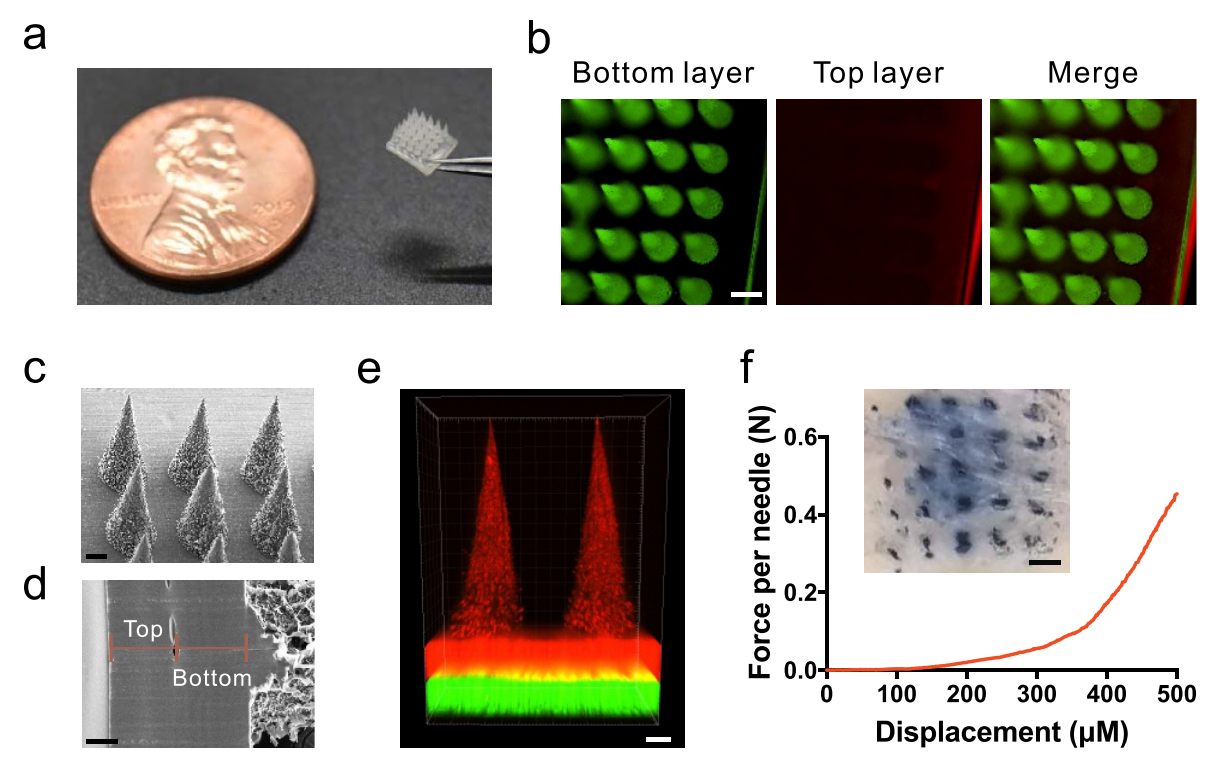


Fig. 2. Transdermal colorimetric microneedle characterization. a) Photo of microneedle array patch next to one cent coin (19 mm in diameter). b) Fluorescence microscopy image showing the extraction layer in green and display layer in red. Scale bar is 500 μ m. A scanning electron microscopy image of c) the colorimetric microneedles (Scale bar, 200 μ m), and d) the intersection of the two layers of the colorimetric patch (Scale bar, 100 μ m). e) The 3D reconstruction of the microneedle patch confocal images with z-direction intervals of 55 μ m using software Imaris. Evenly distributed FITC-labeled GOx and Cy5-labeled HRP-CaP are shown in red and green, respectively. Scale bar, 150 μ m. f) Mechanical strength of microneedles. Inset: excised and trypan blue stained mice skin after insertion of the colorimetric patch (Scale bar, 700 μ m). (For interpretation of the references to color in this figure legend, the reader is referred to the Web version of this article.)

subsequently glued to a pre-formed display patch base encapsulating HRP-CaP and TMB. The as-prepared 4×4 mm patch contains an array of up to 25 (5 \times 5) conical microneedles (Fig. 2a and b). The conical structure of the needle was showed under SEM with base radius of 500 μm , 200 μm spacing, and up to 1500 μm in height (Fig. 2c). We validated the binding affinity of the two layers by imaging the intersection with SEM (Fig. 2d). The two layers have comparable thickness of around 200 nm while hardly any gap could be observed at the interface, suggesting that liquid diffusion and molecular interaction could be achieved between the two layers. Next, we evaluated the GOx and HRP distribution in the bottom and top layer, respectively. A stacked structure with distinguished border could be identified from the 3D reconstruction confocal image of a representative microneedle patch prepared by FITC-labeled GOx and Cy5-labeled HRP-CaP (Fig. 2e). Images show that GOx and HRP-CaP are uniformly distributed in their respective regions of the microneedle patch (Fig. S10 and Video S1).

Supplementary data related to this article can be found at https://doi.org/10.1016/j.biomaterials.2020.119782.

The mechanical strength of the microneedle was determined as 0.45 N at 500 μm displacement using a tensile compression machine, which allows for sufficient skin insertion without breaking. As shown in Fig. 2f, successful penetration of the mouse skin with the microneedle was further demonstrated with staining by trypan blue.

3.3. In vitro test of the glucose-responsive colorimetric sensor

To assess the in vitro color readout of the colorimetric microneedle

in response to different glucose levels, we designed a 4 × 4 mm polydimethylsiloxane (PDMS) based reaction well with a depth of 2 mm to mimic the interstitial fluid extraction process. Each well was filled with 30 µL glucose solutions ranging from 50 mg/dL to 400 mg/dL, just enough to immerse the needle (Fig. 3a). After immersion for 2 min, the needle was taken out and a gradient color change was observed subsequently. A remarkable color difference could be observed within 30 s (Video S2). We performed RGB histogram analysis using ImageJ to provide quantification information of the color display. Instead of analyzing the images captured by cameras, which may require standard light conditions and camera setup, we recorded the color of the microneedle using a regular colored scanner, circumventing the different ambient conditions including brightness, saturation, and shades of the photos taken with cameras (Fig. 3b). With the increase of glucose level, the RGB value dropped with a shifting rate of Red > Blue > Green, contributing to a more cyan color to the naked eye (Fig. 3b and Fig. S11). This characterization provides feasibility of further integrating a smart phone with enhanced precision.

Supplementary data related to this article can be found at https://doi.org/10.1016/j.biomaterials.2020.119782.

3.4. In vivo performance of the transdermal colorimetric glucose sensor

The *in vivo* performance of the colorimetric microneedle sensor was investigated by detecting the hyperglycemia of mice using a mouse model of type 1 diabetes induced by streptozotocin (STZ). In a typical sensing attempt, the microneedle was inserted into the mice's skin and

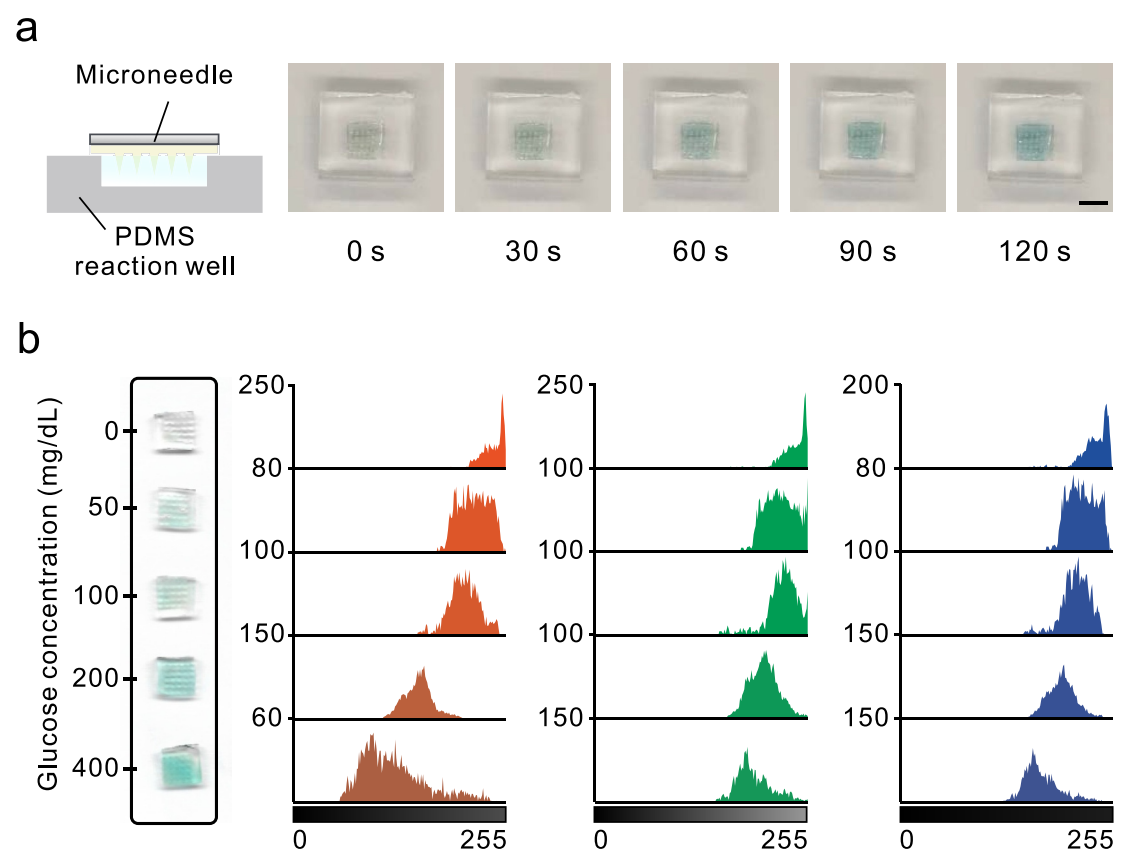


Fig. 3. In vitro color change analysis. a) Schematic and snapshots of the colorimetric patch color change in a polydimethylsiloxane-based well containing 400 mg/dL glucose solution to mimic the interstitial fluid extraction. Scale bar, 4 mm. b) Left: a scanned image showing the color changes of the transdermal colorimetric patches after glucose (50–400 mg/dL) extraction from silicone elastomer well. Right: RGB color histogram of the scanned image, analyzed with ImageJ software. X-axis represents the grey levels of each color channel (Red, Green, Blue), and Y-axis indicates the pixel count number at the corresponding grey level. (For interpretation of the references to color in this figure legend, the reader is referred to the Web version of this article.)

remained in place for 10 min to ensure sufficient extraction of the sample fluid before removal. Meanwhile, the initial colorless patch started to develop a cyan coloration on the hyperglycemic mice and the reaction was completed (Fig. 4a and Video S3). The scanned picture of the removed microneedle patches also revealed a significant decrease in RGB mean values (Fig. 4b and c). As shown in Fig. S12, the removed microneedle has retained structure and bent tips, and the base diameter swelled to 550.7 $\,\pm\,$ 10.4 $\,\mu m$ after insertion, indicating the successful extraction of sample fluid.

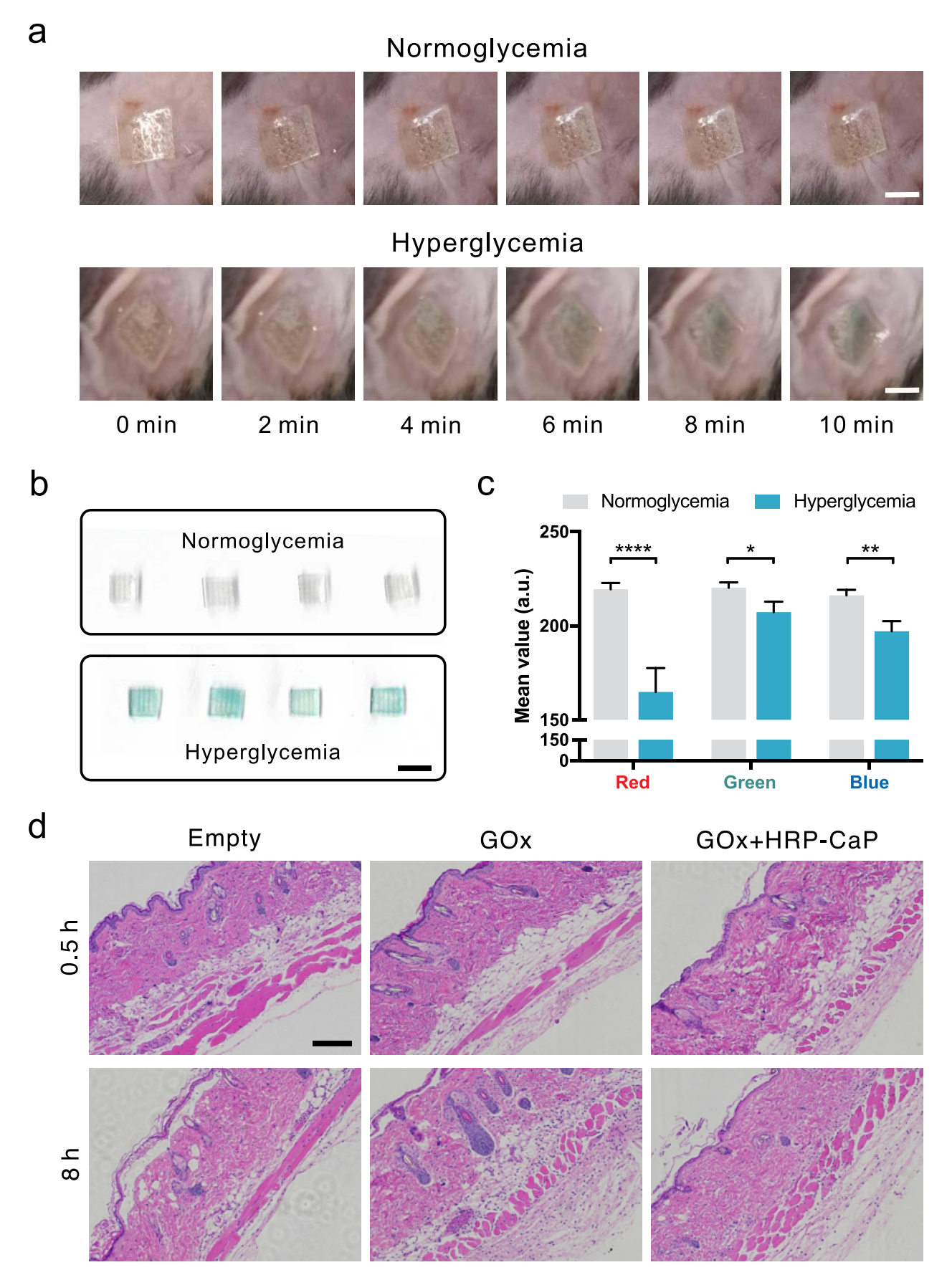
Supplementary data related to this article can be found at https://doi.org/10.1016/j.biomaterials.2020.119782.

For GOx based glucose responsive microneedle systems, excess $\rm H_2O_2$ produced during the process may cause inflammation in the surrounding tissues. Therefore co-loading $\rm H_2O_2$ scavenger such as catalase is necessary for the long-term application of a GOx based microneedle. Hematoxylin and eosin (H&E) staining was performed to elucidate the biocompatibility of the sensor. The results demonstrated that 30 min treatment of empty MN, GOx-MN, and GOx-HRP-CaP colorimetric microneedle showed negligible inflammation (Fig. 4d). This observation may attribute to the relatively short skin contact time of the sensor. An extended insertion time of 8 h caused an obvious neutrophil infiltration in GOx treated skin, reflecting a $\rm H_2O_2$ induced pathophysiological response and tissue damage. However, substantially reduced neutrophil infiltration was observed in the skin of mice treated with

GOx-HRP-CaP microneedle. Here, HRP acts as a $\rm H_2O_2$ consumer to generate color change, which may also alleviate the harm to the surrounding tissues. Furthermore, the colorimetric display part of the sensor is not directly in contact with the skin, eliminating toxicity concerns associated with TMB substrate.

4. Conclusions

In summary, we have presented a glucose colorimetric sensor capable of *in situ* detection of hyperglycemia in mice. Sampling and result display are two important features for practical applications of portable glucose sensors. The double layer microneedle array patch designed with GOx/HRP dual enzyme systems for glucose sensing and color conversion has the potential to achieve both attributes simultaneously. The biomineralization design of HRP takes advantage of the two products from the glucose-glucose oxidase reaction to generate high sensitive detection of glucose level in the interstitial fluid of mice. Meanwhile, the rise in glucose level can be visualized with naked eye and further quantified by analyzing the RGB composition of a scanned picture of the microneedle. This painless and simple to use colorimetric microneedle sensor could be further extended to detect other biomarkers [27] with enhanced patient compliance.



(caption on next page)

Fig. 4. *In vivo* performance study. a) Snapshots of the transdermal colorimetric patch color change *in vivo* at different time points. Scale bar, 3 mm. b) Scanned images of the colorimetric microneedle patches after interstitial fluid extraction from four mice with normoglycemia (100 mg/dL) and hyperglycemia (400 mg/dL). Scale bar, 4 mm. c) RGB mean value of scanned images in b), results are expressed as mean +SD (n = 4). * $^{*}P < 0.05$, * $^{*}P < 0.01$, and **** $^{*}P < 0.001$. d) H&E staining results of skins at the inserted site of mice with treatment time of 0.5 h and 8 h, respectively. Scale bar, 100 μm. (For interpretation of the references to color in this figure legend, the reader is referred to the Web version of this article.)

Declaration of competing interest

The authors declare no conflict of interest.

Author contributions

Z.W. and H.L. contributed equally. Z.W. and Z.G. designed the experiments. Z.W., H.L., J.W., Z.C., G.C., D.W. and A.C. performed experiments and collected data. Z.W. and Z.G. analyzed the data and wrote the paper.

Data availability

The raw/processed data required to reproduce these findings cannot be shared at this time due to technical or time limitations.

Acknowledgements

This work was supported by the grants from National Science Foundation (grant no.1708620), American Diabetes Association (grant no. 1-15-ACE-21), and grant from the start-up packages of UCLA.

Appendix A. Supplementary data

Supplementary data to this article can be found online at https://doi.org/10.1016/j.biomaterials.2020.119782.

References

- [1] A. American Diabetes, Diagnosis and classification of diabetes mellitus, Diabetes Care 27 (Suppl 1) (2004) S5–S10.
- [2] D.M. Nathan, Long-term complications of diabetes-mellitus, N. Engl. J. Med. 328 (23) (1993) 1676–1685.
- [3] D. Bruen, C. Delaney, L. Florea, D. Diamond, Glucose sensing for diabetes monitoring: recent developments, Sensors 17 (8) (2017) 1866.
- [4] R. Paul, A.C. Saville, J.C. Hansel, Y.Q. Ye, C. Ball, A. Williams, X.Y. Chang, G.J. Chen, Z. Gu, J.B. Ristaino, Q.S. Wei, Extraction of plant DNA by microneedle patch for rapid detection of plant diseases, ACS Nano 13 (6) (2019) 6540–6549.
- [5] P. Xue, L. Zhang, Z.G. Xu, J.J. Yan, Z. Gu, Y.J. Kang, Blood sampling using microneedles as a minimally invasive platform for biomedical diagnostics, Appl. Mater. Today 13 (2018) 144–157.
- [6] B. Chua, P.J. Cao, S.P. Desai, M.J. Tierney, J.A. Tamada, A.N. Jina, Sensing contact between microneedle array and epidermis using frequency response measurement, IEEE Sens. J. 14 (2) (2014) 333–340.
- [7] J.C. Yu, Y.Q. Zhang, Y.Q. Ye, R. DiSanto, W.J. Sun, D. Ranson, F.S. Ligler, J.B. Buse, Z. Gu, Microneedle-array patches loaded with hypoxia-sensitive vesicles provide

- fast glucose-responsive insulin delivery, Proc. Natl. Acad. Sci. U.S.A. 112 (27) (2015) 8260–8265.
- [8] W. Chen, R. Tian, C. Xu, B.C. Yung, G. Wang, Y. Liu, Q. Ni, F. Zhang, Z. Zhou, J. Wang, G. Niu, Y. Ma, L. Fu, X. Chen, Microneedle-array patches loaded with dual mineralized protein/peptide particles for type 2 diabetes therapy, Nat. Commun. 8 (1) (2017) 1777.
- [9] Y.C. Kim, J.H. Park, M.R. Prausnitz, Microneedles for drug and vaccine delivery, Adv. Drug Deliv. Rev. 64 (14) (2012) 1547–1568.
- [10] S.R. Corrie, J.W. Coffey, J. Islam, K.A. Markey, M.A.F. Kendall, Blood, sweat, and tears: developing clinically relevant protein biosensors for integrated body fluid analysis, Analyst 140 (13) (2015) 4350–4364.
- [11] A.K. Yetisen, R. Moreddu, S. Seifi, N. Jiang, K. Vega, X. Dong, J. Dong, H. Butt, M. Jakobi, M. Elsner, A.W. Koch, Dermal tattoo biosensors for colorimetric metabolite detection, Angew. Chem., Int. Ed. Engl. 58 (31) (2019) 10506–10513.
- [12] Y. Lin, M. Zhao, Y. Guo, X. Ma, F. Luo, L. Guo, B. Qiu, G. Chen, Z. Lin, Multicolor colormetric biosensor for the determination of glucose based on the etching of gold nanorods, Sci. Rep. 6 (2016) 37879.
- [13] X. Liu, D. Huang, C. Lai, L. Qin, G. Zeng, P. Xu, B. Li, H. Yi, M. Zhang, Peroxidase-like activity of smart nanomaterials and their advanced application in colorimetric glucose biosensors, Small 15 (17) (2019) e1900133.
- [14] E.C. Adams, R.L. Mast, A.H. Free, Specificity of glucose oxidase, Arch. Biochem. Biophys. 91 (2) (1960) 230–234.
- [15] R. Wilson, A.P.F. Turner, Glucose-oxidase an ideal enzyme, Biosens. Bioelectron. 7 (3) (1992) 165–185.
- [16] A.C. Maehly, B. Chance, The assay of catalases and peroxidases, Methods Biochem. Anal. 1 (1954) 357–424.
- [17] D. Jiang, D. Ni, Z.T. Rosenkrans, P. Huang, X. Yan, W. Cai, Nanozyme: new horizons for responsive biomedical applications, Chem. Soc. Rev. 48 (14) (2019) 3683–3704.
- [18] M. Gajhede, D.J. Schuller, A. Henriksen, A.T. Smith, T.L. Poulos, Crystal structure of horseradish peroxidase c at 2.15 angstrom resolution, Nat. Struct. Biol. 4 (12) (1997) 1032–1038.
- [19] K. Chattopadhyay, S. Mazumdar, Structural and conformational stability of horseradish peroxidase: effect of temperature and ph, Biochemistry 39 (1) (2000) 263–270.
- [20] W. Chen, G. Wang, B.C. Yung, G. Liu, Z. Qian, X. Chen, Long-acting release formulation of exendin-4 based on biomimetic mineralization for type 2 diabetes therapy, ACS Nano 11 (5) (2017) 5062–5069.
- [21] Y.R. Cai, Y.K. Liu, W.Q. Yan, Q.H. Hu, J.H. Tao, M. Zhang, Z.L. Shi, R.K. Tang, Role of hydroxyapatite nanoparticle size in bone cell proliferation, J. Mater. Chem. 17 (36) (2007) 3780–3787.
- [22] Z. Wang, Y. Fu, Z. Kang, X. Liu, N. Chen, Q. Wang, Y. Tu, L. Wang, S. Song, D. Ling, H. Song, X. Kong, C. Fan, Organelle-specific triggered release of immunostimulatory oligonucleotides from intrinsically coordinated DNA-metal-organic frameworks with soluble exoskeleton, J. Am. Chem. Soc. 139 (44) (2017) 15784–15791.
- [23] Q. Chang, H.Q. Tang, Immobilization of horseradish peroxidase on nh2-modified magnetic fe3o4/sio2 particles and its application in removal of 2,4-dichlorophenol, Molecules 19 (10) (2014) 15768–15782.
- [24] S.J. Kim, K.J. Lee, I.Y. Kim, Y.M. Lee, S.I. Kim, Swelling kinetics of modified poly (vinyl alcohol) hydrogels, J. Appl. Polym. Sci. 90 (12) (2003) 3310–3313.
- [25] M. Penza, V.I. Anisimkin, Surface acoustic wave humidity sensor using polyvinylalcohol film, Sens. Actuators, A 76 (1–3) (1999) 162–166.
- [26] C.M. Hassan, N.A. Peppas, Structure and morphology of freeze/thawed pva hydrogels, Macromolecules 33 (7) (2000) 2472–2479.
- [27] Y. Xiang, Y. Lu, Using personal glucose meters and functional DNA sensors to quantify a variety of analytical targets, Nat. Chem. 3 (9) (2011) 697–703.